Astron. Astrophys. 358, 499–513 (2000)

ASTRONOMY AND ASTROPHYSICS

ISO observations of a sample of Compact Steep Spectrum and GHz Peaked Spectrum radio galaxies

C. Fanti[1,2], F. Pozzi[3,2], R. Fanti[1,2], S.A. Baum[4], C.P. O'Dea[4], M. Bremer[5], D. Dallacasa[3,2], H. Falcke[6], T. de Graauw[7], A. Marecki[8], G. Miley[9], H. Rottgering[9], R.T. Schilizzi[10], I. Snellen[11], R.E Spencer[12], and C. Stanghellini[13]

[1] Università di Bologna, Dipartimento di Fisica, Via Irnerio 46, 40126 Bologna,Italy
[2] Istituto di Radioastronomia del CNR, Via Gobetti 101, 40129 Bologna, Italy
[3] Università di Bologna, Dipartimento di Astronomia, Via Ranzani 1, 40127 Bologna, Italy
[4] STScI, 3700 San Martin Drive, Baltimore, MD 21218, USA
[5] Bristol University, Department of Physics, H.H. Wills Physics Laboratory, Tyndall Avenue, Bristol, BS8 1TL, UK
[6] Max-Planck-Institut f. Radioastronomie, Auf dem Hügel 69, 53121 Bonn, Germany
[7] Laboratorium voor Ruimteonderzoek, SRON, Postbus 800, 9700 AV Groningen, The Netherlands
[8] Toruń Centre for Astronomy, N. Copernicus University, ul. Gagarina 11, 87-100 Torun, Poland
[9] Sterrewacht, Oort Gebouw, P.O. Box 9513, 2300 RA Leiden, The Netherlands
[10] Joint Institute for VLBI in Europe, Postbus 2, 7990 AA Dwingeloo, The Netherlands
[11] Institute of Astronomy, Madingley Road, Cambridge CB3 0HA, UK
[12] University of Manchester, Jodrell Bank Observatory, Macclesfield, Cheshire SK 11 9L, UK
[13] Istituto di Radioastronomia del CNR, C.P. 141, 96017 Noto (SR), Italy

Received 21 December 1999 / Accepted 10 April 2000

Abstract. We present results from observations obtained with ISOPHOT, on board the ISO satellite[1], of a representative sample of seventeen CSS/GPS radio galaxies and of a control sample of sixteen extended radio galaxies spanning similar ranges in redshift ($0.2 \leq z \leq 0.8$) and radio luminosity ($P_{2.7\mathrm{GHz}} \geq 10^{26}$ W/Hz). The observations have been performed at λ = 60, 90, 174 and 200 μm. The original purpose of these observations was to check whether CSS/GPS sources are associated with very gas rich galaxies, as required by the scenario in which the growth of the radio source is inhibited by the dense medium of the host galaxy.

Unfortunately the resulting performance of ISOPHOT was worse than expected. As a consequence, the detection limit at 60μm is similar to that obtained previously with IRAS but better than that at 90μm.

Seven of the CSS/GPS sources have detections $\geq 3\sigma$ at one or more wavelengths, one of which is detected at $\geq 5\sigma$. For the comparison sample five objects have detections $\geq 3\sigma$ one of which is at $\geq 5\sigma$.

By co–adding the data we have obtained average flux densities at the four wavelengths.

We found no evidence that the FIR luminosities of the CSS/GPS sources are significantly different from those of the extended objects and therefore there is not any support for CSS/GPS sources being objects "frustrated" by an abnormally dense ambient medium.

The two samples were then combined, providing FIR information on a new sample of radio galaxies at intermediate redshifts. We compare this information with what previously known from IRAS and discuss the average properties of radio galaxies in the redshift range 0.2 – 0.8. The FIR emission cannot be accounted for by extrapolation of the synchrotron radio spectrum and we attribute it to thermal dust emission. The average FIR luminosity is $\geq 6 \times 10^{11} L_{\odot}$. Over the observed frequency range the infrared spectrum can be described by a power law with spectral index $\alpha \simeq 1.0 \pm 0.2$. Assuming the emission to be due to dust, a range of temperatures is required, from ≥ 80 K to ≈ 25 K. The dust masses required to explain the FIR emission range from $5 \times 10^5\ M_{\odot}$ for the hotter component up to $2 \times 10^8\ M_{\odot}$ for the colder one.

We present also observations on four nearby ($z \leq 0.1$) GPS radio galaxies, two of which are detected at all four wavelengths.

Key words: galaxies: active – galaxies: ISM – infrared: galaxies – infrared: ISM: continuum – radio continuum: galaxies

1. Introduction

Compact Steep Spectrum (CSS) and GHz Peaked Spectrum (GPS) radio sources are powerful extragalactic radio sources with radio emission confined well within their host galaxy/quasar ($\lesssim 15$kpc)[2]. They are as powerful as the clas-

Send offprint requests to: F. Pozzi
Correspondence to: cfanti@astbo1.bo.cnr.it

[1] Based on observations with ISO, an ESA project with instruments funded by ESA Member States (especially the PI countries: France, Germany, the Netherlands and the United Kingdom) with the participation of ISAS and NASA.

[2] Throughout this paper we use H_0=100 (Km/sec)/Mpc and q_0=0.5.

sical FRII radio sources but are of much smaller physical size and yet have normal/steep radio spectra at GHz frequencies. A discussion of the properties of CSS can be found in Fanti et al. (1990; 1995). A comprehensive and updated review on CSS and GPS is presented by O'Dea (1998).

Some 15 to 25% of sources in a flux density limited sample, depending on the selection frequency, belong to this class. Many of them have radio spectra which show a flattening or a more marked turnover at frequencies between 50 MHz and a few GHz; those sources with a turnover at about 1 GHz are the GPS sources. The turnover is usually attributed to synchrotron self–absorption, but also free–free absorption (Bicknell et al. 1997) and induced Compton scattering (Kuncic et al. 1998) have been considered.

Given that CSS and GPS sources are *physically small*, i.e. of sub–galactic dimensions, it has been suggested that they are either *(1)* young objects (*youth* scenario, Phillips & Mutel 1982), which have yet to develop extended radio lobes or *(2)* sources where the radio emitting plasma is trapped by an unusually dense interstellar medium (*frustration* scenario, van Breugel et al. 1984).

In the latter hypothesis, CSS/GPS radio sources would be as old as those of larger size but their jets would spend their whole lifetime trying to escape, without success, out of the interstellar medium. This scenario requires a rather dense interstellar medium (average density $n_{\rm ISM} \gg 1$ cm^{-3} and total mass within 1 kpc $M_{\rm ISM} > 10^8 M_\odot$; see De Young 1993; Fanti et al. 1995) which is in the path of the radio source. Even if the host galaxy contains a lot of gas, if this is distributed in a disk perpendicular to the radio source axis, it will have little effect on the radio source propagation, therefore any "frustrating" gas has to be distributed over a large volume. Attempts to probe the different phases of this interstellar gas (e.g. optical observations of the Narrow Lines, polarization studies, X–ray emission) have given, in our opinion, little support to the frustration scenario.

Recently, proper motion measurements of the hot spots in a few GPS sources by Owsianik et al. (1998) and Owsianik & Conway (1998) have shown separation velocities $\geq 0.1\ c$. This finding strongly suggests that these sources are very young. Also a recent study of the integrated radio spectra of a number of CSS/GPS (Murgia et al. 1999) provides additional evidence for short lifetimes.

It is nevertheless important to support these recent results with information on the ambient medium around these sources.

The frustration scenario requires that an unusually dense ISM be present in CSS/GPS sources. This may contain a substantial cold phase and a large amount of dust, and, in order to stop the advancing jet, this medium has to have a large covering factor. The dust will therefore absorb and re-process a fraction of the optical and UV radiation from the AGN (and young stars, if present) higher than in the larger size, "non–frustrated", radio sources, giving to the CSS/GPS sources an extra IR emission component in addition to the one from the disk/torus.

Since this dense medium has to extend over several kpc from the nucleus (in order to stop also radio sources 10–15 kpc in size), a large fraction of the dust will be moderately cold so that the emission is expected predominantly in the medium–far IR (MFIR) spectral region.

By searching for emission from cold dust, we have therefore tried to obtain some constraints on this scenario. Since the emission peak is expected at relatively long wavelengths, ISO, with its capability of carrying out photometry at $\lambda \geq 60\mu$m, (Kessler et al. 1996) was well suitable for such an investigation.

This search is better suited to radio galaxies, rather than quasars, as in the former the contamination from the IR emission produced in the innermost regions by the AGN is lower by a factor 4–5 (Heckman et al. 1992). No definitive explanation, within the "unified models" scenario, has yet been given for such a difference (see also Sect. 6.5), but it is an observational effect that we have taken into consideration in planning the experiment. Moreover there are several ISO programs in the Guaranteed Time allocation aimed at observing different samples of quasars, including a number of CSS/GPS, from which the relevant information could be retrieved.

The project of which we present the results is the merging of two independent programs (P.I.s C.F. and H.F.) which both got observing time in the first ISO Call for Proposals. A representative sample of CSS/GPS radio galaxies, unbiased with respect to FIR emission, was selected from various samples of CSS/GPS radio sources. A sample of extended radio galaxies, matched in redshift and radio luminosity, was also selected for observations at the same wavelengths, in order to determine the level of MFIR emission in extended radio galaxies as compared to CSS/GPS galaxies.

The layout of the paper is the following.

Sect. 2 describes the selection of the two samples.

Sects. 3 and 4 describe the ISO observations and the data reduction. In these sections we mention only what is relevant to the paper. For more details we refer the reader to the specific ISO and PIA[3] (*Iso***P***hot* **I***nteractive* **A***nalysis*) literature.

Sects. 5 and 6 present the results and discuss them.

Conclusions are summarized in bf Sect. 7

2. The sample

Eighteen CSS/GPS radio galaxies in the redshift range $0.2 \leq z \leq 0.8$ and with radio size < 10 kpc were originally selected. They are mostly from the 3CR catalogue at 178 MHz (Laing et al. 1983) and from the Peacock & Wall (1982) (PW) catalogue of radio sources at 2.7 GHz, (see Fanti et al. 1995), but some have been selected also from other lists provided the selection was unbiased with respect to IR emission (see Table 1).

Of these radio sources, 3C318 has recently been discovered to be a quasar at a redshift higher than originally believed (Willott et al. 2000) and therefore it has to be dropped from

[3] PIA is a joint development by the ESA Astrophysics Division and the ISOPHOT Consortium led by the Max Planck Institute for Astronomy (MPIA), Heidelberg. Contributing ISOPHOT Consortium institutes are DIAS, RAL, AIP, MPIK, and MPIA.

Table 1. CSS/GPS sample

Source	z	LogP$_{2.7\mathrm{GHz}}$ (W/Hz)	LS kpc	Sample	nominal observing time 60μm sec	90μm sec	174μm sec	200μm sec
0108+38	0.67	26.79	0.023	PW	256	64	128	128
3C49	0.62	26.89	3.6	3CR	192	64	96	128
3C67	0.31	26.30	6.8	3CR	256	128	—	—
0404+76	0.60	27.23	0.53	PW	192	96	96	192
1244+49	0.21	25.63	5.7	San	256	64	128	128
3C268.3	0.37	26.54	3.9	3CR	256	128	32	32
1323+32	0.37	26.75	0.18	PW	192	64	96	96
1358+62	0.43	26.81	0.16	PW	64	32	32	32
3C303.1	0.27	25.60	5.0	3CR	192	96	32	32
1607+26	0.47	26.92	0.18	PW	64	32	32	32
1622+66	0.20	25.66[a]	0.0013	Sn	64	64	64	128
3C343.1	0.75	27.24	1.3	3CR	—	—	32	32
1819+39	0.798[b]	27.23	3.4	PW	192	96	96	96
1819+67	0.22	25.06	0.02	Sn	192	64	32	64
1829+29	0.60	26.96	9.3	PW	64	32	64	128
2342+82	0.74	27.25	0.66	PW	192	64	64	128
2352+49	0.24	26.18	0.15	PW	64	32	64	128
median[d]	0.43	26.79	1.0					
3C318	1.574[c]	27.71	8.2	3CR	64	32	128	192
1345+125	0.12	25.79	0.11	St	64	32	32	64
1718-649	0.014	24.20[a]	0.0014	Tin	256	64	128	128
1934-63	0.18	26.65	0.14	Tzi	—	—	—	64
1946+70	0.10	25.00	0.04	Sn	64	64	64	128

NOTES:
[a] the spectrum of this GPS peaks at ≈3 GHz, and its $P_{2.7\mathrm{GHz}}$ has been extrapolated from the spectrum at high frequencies
[b] revised redshift by Vermeulen et al. (1996)
[c] revised redshift by Willott et al. (2000)
[d] the median values are for the above representative sample ($0.2 \leq z \leq 0.8$)
Sample – PW: Peacock & Wall (1982); 3CR: Laing et al. (1983); San: Sanghera (1995); Sn: Snellen et al. (1998); St: Stanghellini et al. (1997; 1998); Tin: Tingay et al. (1997); Tzi: Tzioumis et al. (1997)

the sample, which counts then 17 CSS/GPS galaxies. However, for completeness, we have included in Table 5 also the data we obtained on this source.

A sample of 16 3CR radio galaxies, with radio sizes > 20 kpc and spanning a similar range in redshift and radio luminosity, was selected for comparison purposes.

The two samples are presented in Tables 1 and 2.

Four additional GPSs, at redshifts < 0.2 were also selected for observations (see Sect. 5.3), although they are not going to be used in the discussion. They also are listed in Table 1, separate from the representative sample.

3. Observations

The sources were observed with ISOPHOT (Lemke et al. 1996), sub–instruments C100 and C200, at the wavelengths of 60, 90, 174 & 200 μm. These wavelengths were chosen in order to cover a spectral range as broad as possible with the best detectors. Actually some sources, mainly in the control sample, were observed in other programmes, including Guaranteed Time Observations, requiring us to observe them only at the wavelengths not planned in the other experiments (see Tables 1 and 2, where the wavelengths missing in our programme are marked by a "—").

The C100 detector consists of a 3×3 matrix of pixels $43.5'' \times 43.5''$ in size and C200 of a 2×2 matrix of $89.4'' \times 89.4''$ pixels. Each pixel is an independent detector, which requires its own calibration.

The diameter of the Airy disks of the Point Spread Functions (PSF) are given in Table 3. By comparison with the pixel sizes, it is clear that for C100 the Airy disk matches approximately one pixel size, while for C200 the PSF covers most of the matrix. Therefore detected sources will be visible mostly on the central pixel #5 with C100, while with C200 the four pixels should give approximately the same values (within the noise). Table 3 gives also the fraction, f_{PSF}, of light falling onto the central pixel (# 5) for C100 and on the four pixels for C200.

Observations were made in *chopper* rectangular mode, with chopper throw 180", in order to have, every few seconds (*chopper plateau*), an ON–source and an OFF–source measure of the

Table 2. Control sample

Source	z	Log $P_{2.7GHz}$ (W/Hz)	LS kpc	nominal observing time 60μm sec	90μm sec	174μm sec	200μm sec
3C16	0.41	26.31	135	64	32	32	64
3C19	0.48	26.77	20	—	—	—	64
3C34	0.69	26.67	174	—	—	—	64
3C42	0.40	26.51	85	—	—	—	64
3C46	0.44	26.18	533	256	64	32	64
3C79	0.26	26.32	212	196	32	128	128
3C274.1	0.42	26.52	470	64	32	32	64
3C277.2	0.77	26.92	214	64	32	64	128
3C284	0.24	25.87	409	64	32	32	32
3C295	0.46	26.51	20	—	—	—	32
3C299	0.37	26.44	33	—	—	—	32
3C330	0.55	27.18	192	—	—	—	32
3C337	0.64	26.96	153	64	32	32	32
3C401	0.20	26.12	40	196	64	32	64
3C441	0.71	27.03	117	64	32	32	128
3C459	0.22	26.18	20	64	32	64	64
median	0.43	26.51	150				

Table 3. Airy disk size, $d_{\rm Airy}$ and $f_{\rm PSF}$ for the filters used in the observations

filter μm	$d_{\rm Airy}$ ["]	$f_{\rm PSF}$	filter μm	$d_{\rm Airy}$ ["]	$f_{\rm PSF}$
C100			**C200**		
60	50.3	0.69	174	134	0.707[a]
90	75.5	0.61	200	168	0.794[a]

[a] Laureijs (1998) – private communication

same time length. The OFF data then have to be subtracted from the ON data, in order to extract the source signal. In this observing mode, the telescope points halfway between the source and the background positions, and a small mirror switches between the two sky positions. This introduces a vignetting error which is different for ON and OFF positions (see Sect. 4).

We applied for and obtained time also in the second "Call for Proposals", mainly for the purpose of increasing the observing time (originally planned on the basis of the ground estimates of the instrument performances). Therefore some of the sources were observed twice.

The total ON–source time ranges from 32 to 256 sec, although the glitch removal and other options of the data reduction (Sect. 4) have shortened the nominal observing time. In Tables 1 and 2 however, we give the total "nominal" ON–source time; for the sources observed twice we give the total.

4. Data reduction

The data analysis was carried on using mainly the PIA V7.2 software (Gabriel et al. 1997). Some further software has been kindly made available to us by Dr. M. Haas from MPIA (Heidelberg) or has been written by ourselves.

PIA removes glitches due to cosmic rays, subtracts the dark current, corrects for drifts, derives the signals from the *ramps*[4], calibrates the data and makes corrections for vignetting.

Special PIA features that we used are:

1) We used the method of ramp subdivision, i.e. we divided each ramp into pieces 0.25 sec long (*pseudo–ramps*) to improve the accuracy of signal determination.

2) to remove glitches we used the "two threshold glitch recognition" which is claimed to work better than the original one. In a number of cases, however, glitch "tails" remain in the data. We wrote a simple IDL program to further statistically remove the glitch residuals. The noise is reduced by approximately a further 20%.

3) Due to "memory effects" the chopper plateaus are not always flat, but in many cases show upwards/downwards trends in the ON/OFF measurements. In absence of an appropriate program which fits these trends and extrapolates the asymptotic value, we used the quite crude PIA option which removes the first half of each chopper plateau, thus cutting in half the observing time.

More detailed remarks on some other of these reduction steps are discussed here below.

4.1. Calibration

The conversion Volt/sec into Watt is made by using an internal calibration source which provides the conversion factors for each of the matrix pixels (or detectors). Then the conversion to Jy

[4] The signal is read from the detector every 1/32 sec and accumulated until the voltage reaches a saturation limit. At this time a "destructive" read–out occurs, which resets the integration. The integral signal between two consecutive destructive read–outs is called a "ramp" and its slope gives the signal in Volt/sec.

is made by using the known instrument and filter characteristics. The flux density scale may still be $\lesssim$ 20% uncertain at 60 and 90 μm (see Sect. 5.2) and perhaps more at 174 and 200 μm.

In addition, the matrices of the OFF measurements are not "flat" after PIA calibration, the pixel–to–pixel fluctuations being much larger than the instrumental noise. This is explained as a residual calibration error of the individual pixels (flat fielding), that we estimate to be up to $\approx \pm 15\%$. This causes fluctuations from pixel to pixel of several tens of mJy, essentially due to the background, as the "true" signal from the sources is rather small. These errors, however, largely cancel out in the (ON – OFF) data and we have not attempted any correction.

Finally, according to the ISO team, it seems that flux densities have to be increased by an amount which depends on the chopper frequency (i.e. the rate at which the chopper switches between ON and OFF positions) and on the signal difference between ON and OFF. At the time of writing this paper this correction has not been firmly established yet, although it is believed to be small for the C200 data. For the C100 data only the strong sources may be affected by this problem (see also Sect. 5.2), while for the average detections (see Sect. 5.4) we expect the correction to be negligible.

4.2. Vignetting corrections

The vignetting corrections applied by PIA have an uncertainty of a few percent. As they are different in the ON and OFF measures, they do not cancel in computing (ON – OFF), as residual flat–field errors do. Given the typical values of the background (Table 4), this uncertainty introduces errors which are not negligible as compared to the source flux densities which are rather weak.

At 60 and 90 μm, pixel # 5, where the source signal is largely concentrated, is not affected by vignetting and the source flux density is safely derived as explained in Sect. 4.3 by dividing the signal on pixel # 5, by the $f_{\rm PSF}$.

At 174 and 200 μm, where the source signal is spread over the four pixels, vignetting errors are a major cause of uncertainty, due to the higher background levels, not only as they increase the final noise, but also as they introduce systematic effects. Indeed, after application of PIA vignetting corrections, we got the peculiar result that the (ON – OFF) flux densities were, on average, systematically negative, with a clear dependence on the background brightness. This effect is very likely due to residual vignetting errors.

We have therefore tried to estimate such corrections independently, from our own data. For this purpose we used a method suggested by Dr. M. Haas, from MPIA, whose application we take the responsibility for. We assumed that the pixels which are more central with respect to the telescope pointing, i.e. # 2 and #3 at ON, and # 1 and #4 at OFF position, are, at the first order, unaffected by vignetting, while the other pixels are.

As the PSF fills essentially all four pixels, they do see the same signal. Any deviation from this is attributed to vignetting. Considering only the sources with very strong background ($\gtrsim$20 MJy/ster), assuming that the source signal is negligible as compared to the background, and that the background does not change appreciably from ON to OFF, the four pixels at ON position ought to see approximately the same signal as the four pixels at OFF. Therefore the ratios of the signal in pixels # 1 and # 4 ON (assumed to be the only ones affected by vignetting) to the signal of the corresponding pixels at OFF position (assumed to be unaffected by vignetting) give the vignetting errors for these two pixels. The same procedure is applied to pixels # 2 and #3 at OFF position. Note that flat–fielding errors cancel out in taking the ratios of corresponding pixels.

The correction factors deduced from the different sources are consistently in the range from 3% to 5% and were applied to all the sources. The estimated residual uncertainty is $\approx$ 1.0%. The application of these corrections eliminates the problem of the systematic negative (ON – OFF) values and of their dependence on the background brightness.

Table 4. Noise, confusion and total flux density errors

λ μm	$\sigma'_{\rm n}$(64 sec) mJy/pix	$\sigma'_{\rm cc}$ mJy/pix	bckg MJy/sr	$\sigma'_{\rm egc}$ mJy/pix	$\sigma_{\rm T}$ mJy
60	27	9	(2)	2	42
90	12	5	(2)	4	22
174	23	8	(10)	22	148
200	61	6	(20)	23	195

Values in parentheses are the background brightness at which $\sigma'_{\rm cc}$ is computed

4.3. Flux density determination

For C100 the source flux density should be derived by fitting a PSF of known width to the (ON – OFF) matrix values. In practice our signal is always very weak and will only be detectable on pixel #5. Therefore we have computed the source flux density simply by dividing the flux density falling onto pixel #5 by the appropriate value of $f_{\rm PSF}$ given in Table 3.

For C200 the flux density has been obtained by summing the (ON–OFF) four matrix pixels and dividing the result by the $f_{\rm PSF}$ in Table 3.

In the following we shall therefore use as units *mJy/pixel* to refer to the flux density falling onto *one single* pixel and *mJy* to indicate source flux density.

4.4. Estimate of statistical flux density errors

Besides the calibration and vignetting errors, additional uncertainty in the flux density measurements is caused by: *a)* instrumental noise (or simply *noise*, $\sigma_{\rm n}$), which includes all noise contributions along the signal chain (i.e. photon noise due to source and background, plus detector noise), *b)* confusion due to foreground galactic *cirrus* ($\sigma_{\rm cc}$) and *c)* confusion due to extragalactic background ($\sigma_{\rm egc}$). Typical values are reported in Table 4.

In the next paragraphs we discuss how they have been evaluated in the paper.

a) Instrumental noise, $\sigma_{\rm n}$

The nominal instrumental noise *per pixel* is given by the equation:

$$\sigma'_{\rm n} = \sqrt{NEP^2_{\rm source} + 2NEP^2_{\rm bck} + 2NEP^2_{\rm rec}} \quad (1)$$

where the NEP's are the **N**oise **E**quivalent **P**ower of source, background and receiver, to be computed using parameters given in the ISO manuals and which depend on the ON–source time. The factors of 2 in Eq. (1) derive from the fact that the signal is obtained from (ON – OFF) measurements. From the values of the parameters necessary to compute the NEP's it is clear that, except for very high backgrounds ($\gtrsim 100$ MJy/ster) or for very strong sources ($\gtrsim$ 50–100 Jy), the contribution of the detector to the nominal noise is expected to dominate.

Because the resulting performance of the instrument was worse than expected, we adopted a pragmatic method and estimated $\sigma'_{\rm n}$ from the data themselves, instead of using the parameters given in the manuals.

To estimate $\sigma'_{\rm n}$ directly from the data, within each observation we used the chopper sequence (i.e. the sequence of ON–OFF pairs of each source) to determine the statistics of the (ON – OFF) values. For C100 we used only pixel # 5, thus avoiding the residual flat–field (Sect. 4.1) and vignetting (Sect. 4.2) problems. For C200 we used the four pixels together, after application of vignetting corrections, and ignoring the residual flat–field corrections.

The average (ON – OFF) gives the flux density within pixel # 5 for C100 and the flux density within any of the four pixels for C200. The r.m.s. distribution of the ON–OFF pairs gives the "actual instrumental noise" $\sigma'_{\rm n}$ (in mJy/pixel) of *that one* observation. The software for this analysis is due to M.Haas (private communication).

We find that $\sigma'_{\rm n}$ can change significantly from source to source, even for similar backgrounds and observing times. The *median* values, however, scale rather well with the inverse of the square root of the ON–source time. We do not find any difference as a function of the background brightness, which confirms that the detector noise is the dominant factor. The noise computed in this way is in agreement with that from Eq. 1 when adopting the parameters of the ISO manual, except for $\lambda = 200\mu$m where our estimate is lower. This proves, to us, that no significant systematic error is present in our data and that glitches have been removed fairly well.

Given the good behavior of the instrumental (mostly detector's) noise with $1/\sqrt{t}$, we give in Table 4, for each observing wavelength, one single value for $\sigma'_{\rm n}$, corresponding to an integration time of 64 sec. Note that with C200, since the four pixels are independent detectors, the flux density error due to the noise will be computed as $\sigma_{\rm n} = 2 \times \sigma'_{\rm n}/f_{\rm PSF}$.

b) Cirrus confusion noise, $\sigma_{\rm cc}$

This term has been evaluated by Gautier et al. (1992) who provide useful tables to compute $\sigma_{\rm cc}$ on any angular scales (3 arcmin, in our case, the value of the chopper throw) and also show that cirrus confusion depends strongly on the galactic background brightness, B, according to $\sigma_{\rm cc} \propto B^{1.5\pm0.2}$.

Since our measurements include a contribution from the celestial fore/back–grounds and, at least at 60 and 90 μm, a strong contribution from zodiacal light, in order to estimate, $\sigma'_{\rm cc}$ (within a pixel), at all four wavelengths, for both C100 and C200 we used IRSKY software by IPAC which applies a model to remove the zodiacal light, providing also the values for a pure galactic foreground. This estimate of $\sigma'_{\rm cc}$ is accurate to within a factor of two.

Note that, for $\lambda > 100\mu$m, the foreground provided by IRSKY is extrapolated from the IRAS shorter wavelengths, using the dust emission model by Desert et al. (1990). This increases the uncertainty on $\sigma'_{\rm cc}$. For consistency and to be conservative we generally used the IRAS background, which is, on average, higher than ISO's, except in those cases in which, by comparison with the other satellite values, the extrapolation from IRAS was obviously wrong. In those cases we used the ISO background.

We have also compared IRSKY values of $\sigma'_{\rm cc}$ with those reported in ISO manuals: while at 60 and 90 μm the two estimates do agree, at $\lambda = 174\mu$m the ISO manual estimate is over one order of magnitude greater than IRSKY's. We found no estimate at 200μm.

As a reference, we report in Table 4 the values of $\sigma'_{\rm cc}$ at each wavelength, from IRSKY, for a foreground brightness typical of our observations.

c) Extragalactic confusion noise, $\sigma_{\rm egc}$

This is simply due to the piling up, within a beam, of faint galaxies not individually resolved by the instrument. The estimate of the magnitude of this effect, within each pixel, is reported in Table 4 and is derived by IRSKY, in the hypothesis of cosmological evolution of faint galaxies. These values are about a factor of two higher than in the case of a non–evolving model.

Note that with C200, since the PSF covers most of the four pixels, we considered the cirrus and extragalactic confusion correlated across the matrix and therefore we adopted, as the flux density error, $4\times$(pixel error)/$f_{\rm PSF}$.

The total error on source flux density is then computed as:

$$\sigma_{\rm T} = \sqrt{\sigma^2_{\rm n} + \sigma^2_{\rm egc} + \sigma^2_{\rm cc}} \quad (2)$$

where $\sigma_{\rm n}$ is the *individual source* noise, $\sigma_{\rm egc}$ is the error due to the extragalactic confusion (which is the same in all fields at a given wavelength) and $\sigma_{\rm cc}$ the cirrus confusion noise appropriate for the specific source background (zodiacal light subtracted). In Table 4 total flux density errors, appropriate to the parameters in the Table, are also given as an example.

As it can be seen from Table 4, the extragalactic source and cirrus confusion ($\sigma_{\rm egc}$ and $\sigma_{\rm cc}$) may be not negligible as compared to the instrumental noise and may limit the instrument sensitivity considerably or lead to spurious detections, as it will be further discussed in Sect. 5.1.

As an internal test, we used those sources observed twice (with different backgrounds) to check the goodness of error evaluation.

At each wavelength, we compared the difference ΔS of the two measured flux densities with the combined total error ($\sigma^c_{\rm T}$)

Table 5. Sources detected at different levels of reliability (mJy)

	Source	$\lambda = 60\ \mu$m			$\lambda = 90\ \mu$m			$\lambda = 174\ \mu$m			$\lambda = 200\ \mu$m		
		S	$\sigma_{\rm n}$	$\sigma_{\rm T}$	S	$\sigma_{\rm n}$	$\sigma_{\rm T}$	S	$\sigma_{\rm n}$	$\sigma_{\rm T}$	S	$\sigma_{\rm n}$	$\sigma_{\rm T}$
$*$	3C49	42	14	15	16	17	23	335	52	146	*623*	102	155
	1244+49	22	18	21	36	16	17	187	48	133	55	134	177
$*$	1323+32	1	16	17	*45*	11	13	187	36	130	306	108	157
$*$	3C303.1	–2	18	23	45	17	19	*543*	117	172	368	248	274
$*$	1622+663	77	30	33	*43*	8	12	–85	73	145	81	89	146
$**$	1819+39	*91*	19	21	**147**	6	12	33	53	136	8	132	176
	1829+29	99	40	51	129	36	80	–741	44	313	–348	107	171
$*$	2352+49	8	59	61	66	27	51	204	47	343	*655*	130	202
$*$	3C318	*118*	35	36	*104*	21	24	277	60	150	239	68	135
$**$	1345+125	**1470**	45	46	**1171**	23	24	**1273**	119	172	**1471**	287	310
$**$	1718–64	**499**	27	33	**602**	13	44	**2331**	41	396	**2216**	77	184
	1946+70	56	49	51	10	11	41	–28	52	334	433	105	184
	3C16	–77	33	44	–16	25	33	181	47	164	393	156	197
$*$	3C34										*781*	149	193
	3C46	11	17	17	32	10	13	283	115	177	212	162	200
$*$	3C79	66	24	29	37	14	37	378	29	326	*625*	103	181
$*$	3C277.2	*87*	25	27	–18	13	16	289	42	133	207	152	191
$*$	3C284	*179*	47	47	18	29	30	51	150	197	86	180	214
	3C401	2	14	17	32	18	22	238	55	158	469	213	244
	3C441	5	28	30	–7	19	29	11	80	246	453	120	178
$**$	3C459	**698**	44	51	**747**	45	48	*668*	43	157	**1164**	157	196

flux densities in **bold** characters are those for which $S > 5 \times \sigma_{\rm T}$;
flux densities in *italic* characters are those for which $3 \times \sigma_{\rm T} \leq S \leq 5 \times \sigma_{\rm T}$

obtained by adding in quadrature the $\sigma_{\rm T}$ of the two observations. If errors are estimated properly, the ratio $\Delta S/\sigma^c_{\rm T}$, computed for all the available pairs, should have zero average and standard deviation =1.

In spite of the very poor statistics (8 sources observed twice with C100 and 4 with C200) the agreement is satisfactory.

5. Results

5.1. Individual detections

About half of the observed radio galaxies, both in the representative sample of CSS/GPS and in the comparison sample, have $S > 3 \times \sigma_{\rm n}$, at least at one wavelength. These could be considered "formal" detections, in the sense that we got *some signal* out of the instrumental noise. This *does not mean*, however, that we have *detected our target sources*, since, as seen in Table 5, extragalactic and/or cirrus confusion could cause spurious detections: we might just have detected a cirrus filament or a fluctuation in the confusion.

We have checked the reality of these "formal" detections by looking for "negative" detections. We have only three such cases (see Tables 5 and 6) suggesting that, after all, in the "formal" detections some signal from the target is present. This is why we have kept them in Table 5. The test for "claiming" a detection, however, is made by comparing S with $\sigma_{\rm T}$ (Eq. 2).

We considered **detected** the sources for which $S \geq 5 \times \sigma_{\rm T}$ at least at one wavelength (value in **bold** in Table 5) and *possibly detected* those for which $3 \times \sigma_{\rm T} \leq S < 5 \times \sigma_{\rm T}$ (value in *italic* in Table 5).

Table 5 gives the detected, possibly detected and "formally" detected sources, listing the flux densities at all four wavelengths (significant or not) and related errors. The sources detected at least at one wavelength are marked with $**$; those possibly detected are marked with $*$. In each column we give $S, \sigma_{\rm n}$ and $\sigma_{\rm T}$ in mJy (1 σ level).

In Table 5 only two sources from the representative (1819+39) and control (3C459) samples are clearly detected at least at one wavelength. Nine more sources have flux densities which exceed 3 $\sigma_{\rm T}$, but are $<$ 5 $\sigma_{\rm T}$, and are therefore possible detections.

The quasar 3C318 is detected at a $\geq 3\sigma$ level at both 60 and 90 μm.

We also detect clearly at all four wavelengths two of the four nearby GPS (1345+125 and 1718–64).

In Table 6 we list the undetected sources with their S, $\sigma_{\rm n}$ and $\sigma_{\rm T}$, in mJy.

5.2. Comparison with IRAS data

As stated in the *IRAS Explanatory Supplement* (1985) the sensitivity limits (3σ) of the all–sky survey for point sources (PSC)

Table 6. Undetected sources (mJy)

Source	$\lambda = 60\ \mu$m			$\lambda = 90\ \mu$m			$\lambda = 174\ \mu$m			$\lambda = 200\ \mu$m		
	S	$\sigma_{\rm n}$	$\sigma_{\rm T}$	S	$\sigma_{\rm n}$	$\sigma_{\rm T}$	S	$\sigma_{\rm n}$	$\sigma_{\rm T}$	S	$\sigma_{\rm n}$	$\sigma_{\rm T}$
0108+389	9	19	19	5	11	14	45	40	149	242	106	158
3C67	–2	12	18	28	13	33						
0404+76	7	37	39	–14	18	33	–645	95	286	–217	170	220
3C268.3	17	22	24	2	15	17	34	57	137	151	224	252
1358+624	54	30	31	22	29	30	124	168	210	222	213	243
1607+26	71	60	62	83	43	45	–11	122	181	302	223	252
3C343.1							–175	84	152	–151	102	154
1819+670	23	13	16	–26	27	29	23	86	157	–55	199	231
2342+82	–3	30	33	32	14	36	–68	81	329	0	219	265
1934–63										40	93	154
3C19										630	229	256
3C42										348	132	179
3C274.1	53	49	54	–18	32	33	6	71	144	–237	128	173
3C295										–111	102	154
3C299										358	148	188
3C330										191	246	272
3C337	–21	33	34	43	17	18	–141	58	138	353	192	224

Table 7. Available IRAS flux densities (mJy)

Source	60μm	100μm	ref.
3C79	179±9	<330	1
1345+125	2098	1738	2
3C318	170±26	300±70	1
3C459	683	708	2

ref: 1) Heckman et al. (1992); 2) Golombek et al. (1988)

are quite high ($\sim$0.5 Jy at 60 μm and 1.5 Jy at 100μm) but can be sensibly reduced by co–adding several scans, as done, for instance by Heckman et al. (1992; 1994), who obtained 3σ detections on individual objects of $\approx$100 and $\approx$400 mJy at 60 μm and 100μm respectively. The most sensitive IRAS observations were obtained by pointed observations (see e.g. Neugebauer et al. 1986; Golombek et al. 1988). The resulting noise varies from field to field and is typically in the range of 50–100 mJy (3σ) at 60μm and 100–300 mJy (3σ) at 100μm. These values have to be compared with our typical 3σ errors, given in Tables 5 and 6, of $\approx$90 mJy at 60 μm and $\approx$75 mJy at 90μm (median values). Therefore, while at $\lambda = 60\mu$m ISO is not much more sensitive than IRAS, at $\lambda = 90\mu$m the situation is improved.

We searched the literature to see whether any of the sources in our sample has been detected by IRAS at any wavelength. The galaxies from our lists detected by IRAS at 60 and/or 100 μm are reported in Table 7.

On the strongest source (1345+125) about 30% of the IRAS flux density is missing in our observations. This is the case where chopper frequency corrections, that we have not applied (Sect. 4.3), are expected to be larger. For 3C459, which is not as strong, the agreement with the IRAS data is rather good. We are therefore confident that the missing correction is definitely minor for the fainter sources and negligible for the median flux densities that we report. For the fainter sources, we note that 3C79 is possibly detected in our observations only at wavelengths longer than 100μm and that 3C318 at 90 μm is fainter than in IRAS, although the two flux densities are still within $\sim$ 2.5 of the combined errors.

Conversely 3C284 possibly detected (3.8 σ level) at 60 μm in our ISO observations, has only an upper limit in IRAS (Impey & Gregorini 1993) not too different from our measurement. The remaining sources detected (1819+39) or possibly detected at 60 and/or 90 μm by ISO, are weaker than the IRAS upper limits (Heckman et al. 1994).

5.3. Comments on some individual sources

1345+125.

This radio source is identified with a galaxy with "two nuclei", of which the western one has an optical spectrum consistent with Narrow Line radio galaxies and Seyfert type II (Gilmore & Shaw 1986). There is some confusion in the literature about which of the two hosts the radio source. Gilmore & Shaw (1986) and Baum et al. (1988) indicated the eastern (non Seyfert nucleus). More recently, however, Capetti (1998, private communication), Stanghellini et al. (1998) and Evans et al. (1999) presented convincing evidence for the association of the GPS source with the western Seyfert nucleus. This double nucleus galaxy is considered a merger which has triggered the radio activity (e.g. Heckman et al. 1986; Sanders et al. 1988; Surace et al. 1998). Although the optical spectrum is characterized by Narrow Lines, broad Paα (FWHM ~ 2600 km s^{-1}) is seen in the near-IR (Veilleux et al. 1997). In addition, Hurt et al. (1999) report HST/FOC ultraviolet observations which show extended polarized UV continuum light. Both the UV polarization and

the broad Paα indicate that 1345+125 has a hidden (but not too deeply hidden) quasar. This is the first GPS radio galaxy detected in X-rays ($L_{\rm X(2-10Kev)} \approx 2 \times 10^{43}$erg s^{-1}, O'Dea et al. 2000).

We estimate a temperature of $\sim$ 30 K and a dust mass of $\sim 3.5 \times 10^8$ M$_\odot$ for the component which makes the dominant contribution to our ISO data (Table 10). Although our ISO observations are not sensitive to gas at temperatures below about 25 K, the CO observations are sensitive to gas with kinetic temperatures to within a factor of a few of the microwave background temperature (e.g. O'Dea et al. 1994; Allen et al. 1995). For a standard Galactic gas/dust ratio of 100 this corresponds to a mass of molecular gas $\sim 3.5 \times 10^{10}$ M$_\odot$ which is in good agreement with the estimate derived from CO observations ($\sim 3 \times 10^{10}$ M$_\odot$, Mirabel et al. 1989; Evans et al. 1999). This agreement between the ISO and CO estimates of the molecular gas mass may be fortuitous since the gas-to-dust ratio may vary between galaxies and in general is not well determined (e.g. Goudfrooij et al. 1994; Falco et al. 1999).

3C 318

This object was classified as an N–galaxy at a redshift 0.75 by Spinrad & Smith (1976) and considered to be a Narrow Line (NL) radio galaxy by Hes et al. 1995. Recently Willott et al. (2000), from UKIRT spectroscopic observations, detected broad H$_\alpha$ and revised the redshift at 1.574. The object is now classified as a quasar. It is a strong X–ray emitter (Taylor et al., 1992) with a luminosity, updated for the new redshift, of $L_{\rm X(0.5-4.5Kev)} \approx 8 \times 10^{44}$erg s^{-1},

1622+663

This object has a broad a H$_\alpha$ line. It can be classified as a Seyfert 1.5 (Snellen et al. 1999). Its broad–line region seems to be heavily obscured. It is marginally detected at 90 μm.

1718–649

The source is identified with the 12.6 blue magnitude galaxy NGC 6328 (Savage 1976), whose nucleus has a LINER type optical spectrum (Fosbury et al. 1977). The galaxy is quite peculiar, having the appearance of a high luminosity elliptical with faint outer spiral structure and containing a large amount of atomic hydrogen (Veron-Cetty et al. 1995). The object is regarded as a merger of two galaxies, at least one of which is a gas-rich spiral, in the process of forming an elliptical. A very strong source (a star?) is listed in the IRAS PSC, at 3.7 arcmin from 1718–649. Inspection of IRAS maps at 60 and 100 μm shows a fainter extension of this bright source to the North, at the position of 1718–649.

The dominant component of dust contributing to our ISO detection has an estimated temperature of 20 K and a mass of $\sim 0.1 \times 10^8$ M$_\odot$ (Table 10) which would correspond to a gas mass of $\sim 10^9$ M$_\odot$. This is at least an order of magnitude less than the mass of HI ($\sim 3.1 \times 10^{10}$ M$_\odot$, Veron-Cetty et al. 1995). The HI is distributed over the entire galaxy and much of it lies in a partial ring with a diameter of 95" (19 kpc). Possibly, much of the dust in this object lies at large distances from the nucleus and is relatively cold, thus escaping detection in our ISO observations. CO observations would be useful.

1819+39

Its redshift has been re–measured by Vermeulen et al. (1996) who also show that this object has broad H$_\beta$. Thus, this object appears to be Broad Line radio galaxy.

1934–638

The radio source is associated with the brighter galaxy of a pair of compact galaxies ($\approx$ 8 kpc separation) sharing a common envelope (Jauncey et al. 1986). Fosbury et al. (1987) suggest larger amounts of gas and dust than generally found in typical Narrow Line radio galaxies. Tadhunter et al. (1994) found presence of polarized light, suggesting an anomalous environment (see also Morganti et al. 1997). It is undetected at the only observed wavelength (200 μm).

1946+70

This is one of the three GPS sources from the sample of Snellen et al. (1998), and it is much weaker than those from the 3CR and PW samples. It is "formally" detected at 200μm.

3C459

The optical object has been classified as N–galaxy by Spinrad et al. (1985). It was studied in detail at radio and optical frequencies by Ulvestad (1985), who concluded that this galaxy may have undergone a large amount of fairly recent star formation. Hes et al. (1995) classified it as Narrow Line radio galaxy and suggest that a fraction of the FIR emission may be due to heating of the dust by the moderately young blue stars.

5.4. Average detections

We have looked for "statistical" emission from both the representative CSS/GPS sample (i.e. for $0.2 \leq z \leq 0.8$) and the control sample. We have computed both the mean and the median flux density, although in the following we use the second one, which is considered to be more robust since it is less affected by extreme flux density values. In computing the mean flux density we excluded 3C459 for C100, since its large detected flux density would affect the results too much (the source was used, instead, in computing the median).

Values are given in Table 8. The uncertainty on the mean and median are derived from the flux density distribution itself. Note that, as the error distribution of the median is not Gaussian, we choose to give the 95% confidence uncertainty, equivalent to a 2 σ limit for a Gaussian distribution. To make the comparison easier we then give 2σ errors also on the mean.

Table 8. Average flux densities for the CSS/GPS and the comparison sample

λ	CSS/GPS		Control	
	mean	median	mean	median
μm	mJy		mJy	
60	36±24	20^{+34}_{-13}	34±48	32^{+55}_{-30}
90	39±22	34^{+11}_{-18}	11±18	25^{+15}_{-40}
174	–2±156	34^{+90}_{-119}	198±146	210^{+90}_{-195}
200	140±130	116^{+186}_{-116}	370±168	355^{+120}_{-145}

errors on both mean and median are 2 σ (see text)

Table 9. Average flux densities and FIR luminosities for the whole sample

λ	mean	median	$L_{FIR}/L_\odot$	L_{FIR}
μm	mJy			erg s^{-1}
60	35±22	20^{+34}_{-13}	6×10^{10}	$\approx 2.4\times10^{44}$
90	29±16	32^{+15}_{-16}		
174	74±114	48^{+139}_{-37}	$\approx 10^{11}$	$\approx 5\times10^{44}$
200	256±112	232^{+123}_{-114}		

errors on both mean and median are 2 σ

At 60 and 90 μm there is clearly a 3 σ detection for the CSS/GPS sample. In the comparison sample, where the statistics is poorer, as we do not yet have data for $\approx 1/3$ of the objects (see Table 2), both mean and median flux densities, compared with the errors, do not indicate a significant detection. They are, however, largely consistent with the CSS/GPS results. This is reinforced by a comparison done with Heckman et al. (1992; 1994). These authors give co–added flux densities for a sample of radio galaxies. In their "near sub–sample" ($0.3 \lesssim z \lesssim 0.85$, median $z = 0.48$), composed of 5 CSS/GPS and 36 large size sources, and therefore similar to our comparison sample, the median flux densities ($S_{60} \approx 25\pm5$ mJy, $S_{100} \approx 40\pm12$) are consistent with ours, but have smaller errors, due to the much larger number of sources in their sample.

At 174μm and 200μm radio galaxies in the control sample seem stronger FIR emitters, although the difference is not significant at either wavelength. Averaging the two wavelengths the difference is around 2σ.

We have also applied a Kolmogoroff–Smirnov test, which shows that the hypothesis that the two galaxy samples are extracted from the same population is acceptable at a 99% confidence level at all wavelengths.

Considering also the results from Heckman et al. (1992; 1994), we estimate that any IR excess for CSS/GPS sources does not exceed (at a 95% confidence level) $\sim$ 25 mJy in the range 60–90 μm and $\sim$ 100 mJy in the range 170–200 μm.

Our first conclusion then is that we do not have any statistical evidence that the MFIR properties of the galaxies associated with CSS/GPS sources are much different from those of the galaxies associated with large size radio sources (see also Sect. 6.2) consistent with the results of Heckman et al. (1994). The small and large sources we observed seem to have similar average luminosities at all four wavelengths, and hence a similar spectrum between 60 and 200 μm (observer frame). This will allow us to combine the two sets of data in the discussion (Sect. 6.2).

6. Discussion

6.1. FIR tail of synchrotron emission

We have collected all the flux densities available in the literature at radio wavelengths for every source in the sample. No evidence is seen for bright flat spectrum cores at the highest available frequencies (often up to 230 GHz, 1300 μm). The spectra can be well fitted either with a power law or with a model which includes spectral curvature due to synchrotron losses (see Murgia et al. 1999, for details). For each source, using the fitted spectrum, we have extrapolated the flux densities at 60, 90, 174 and 200 μm. The extrapolated average synchrotron flux density is very small ($\lesssim$ 2 mJy at 200 μm and less at the other wavelengths) and does not contribute significantly to the FIR emission. Therefore we attribute the emission we find to genuine thermal radiation.

6.2. FIR luminosities of the combined *CSS/GPS and comparison sample*

As discussed in Sect. 5.4, our data do not show any statistically significant evidence for differences in the FIR luminosities of CSS/GPS and large size radio galaxies at 60 and 90 μm, the situation being somewhat more uncertain in the 174–200 μm interval.

Now we combine the two samples together into a single *sample of powerful radio galaxies at intermediate redshift* to be studied on its own, independent of the type of associated radio source. In Table 9, we report the mean and median FIR flux densities of the combined sample and the average FIR luminosities in the 60–90μm and 174–200 μm ranges.

The FIR luminosities from the median values of the whole sample are calculated as:

$$L_{\rm FIR} = 4\pi D_{\rm L}^2 \nu S_\nu$$

where S_ν is the median flux density at the frequency ν and $D_{\rm L}$ is the luminosity distance.

The average $L_{\rm FIR}$ are in the range $(0.6-1.0)\times10^{11}\ L_\odot$, or (2–5)$\times10^{44}$ erg s^{-1}. The brightest objects, 1819+39 and 3C459, which are several times more luminous than average (Table 10), have peculiarities, as commented in Sect. 5.3, which may well account for their larger FIR luminosities.

These luminosities are much higher than those found in nearby radio quiet elliptical galaxies, which are in the range of up to $\approx 10^8 L_\odot$ (Goudfrooij & de Jong 1995; Bregman et al. 1998).

Table 10. Luminosities and dust masses for the bright sources

Source	Log($L_{FIR}/L_\odot$)		Hot Component		Cold Component	
	60–90μm	174–200μm	T(K)	Mass($M_\odot$)	T(K)	Mass($M_\odot$)
1345+125	11.6	12.2	70	4.4×10^6	30	3.5×10^8
3C 318	12.1	–	100	8×10^6	–	–
1718–64	9.3	9.5	60	2.9×10^4	20	0.1×10^8
1819+39	12.2	–	65	1.5×10^7	–	–
3C 459	11.9	11.5	70	4.6×10^6	25	3.7×10^8

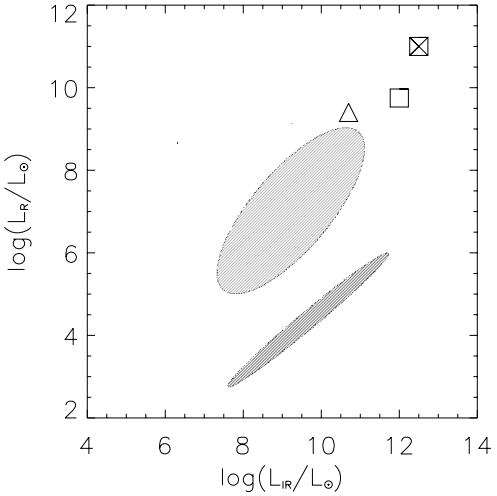

Fig. 1. Radio versus IR luminosity. Shaded areas represent the regions occupied by spirals (*below*) and low power radio galaxies (*above*) from Knapp et al. (1990). The triangle marks the median values for the present sample of radio galaxies, while the empty and crossed squares are the low$-z$ and high$-z$ quasars respectively (Heckman et al. 1992)

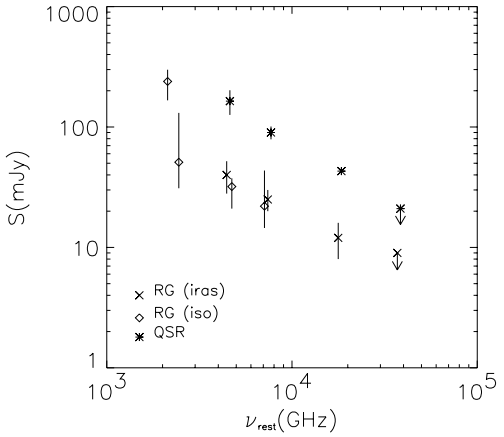

Fig. 2. IR spectrum of radio galaxies (*crosses*: IRAS, *diamonds*: ISO) and quasars from Heckman et al. (1992) (*asterisks*). Error bars are 1 σ

We point out that the median FIR luminosity we find follows the extrapolation of the $L_{\rm FIR}$ vs $L_{\rm radio}$ plot for nearby radio galaxies presented in Knapp et al. (1990) (see Fig. 1).

6.3. Temperature and dust masses

On the hypothesis that the dust is transparent at these wavelengths, the MFIR radiation due to dust at a uniform temperature T follows a modified Planck law given by

$$S(\nu_0) = \frac{\mu(\nu_e) B_{\rm b.b.}(T,\nu_e) M_{\rm dust}(1+z)}{D_{\rm L}^2} \qquad (3)$$

where ν_0 and ν_e are the observed and emitted frequencies, μ is the absorption coefficient, $B_{\rm b.b.}$ is the brightness of a black body at temperature T, $M_{\rm dust}$ is the dust mass, $D_{\rm L}$ is the luminosity distance and z is the source redshift. The absorption coefficient is rather uncertain. In order to keep consistency with the values generally assumed in the literature (e.g.: Hildebrand 1983; Knapp et al. 1990), we take $\mu(\lambda) = 10 \times (250/\lambda(\mu m))$ for $\lambda \leq 250\mu$m. With respect to other assumed values, this tends to overestimate the dust mass (e.g. by a factor of two as compared to the $\mu(\lambda)$ assumed by Hughes et al., 1997).

The MFIR average spectrum for our sample is shown in Fig. 2. In order to describe it better, we used also the following additional upper limits or median flux densities: <5 mJy at 1.3 mm (230 GHz), as maximum flux density excess over the extrapolated synchrotron spectrum (Murgia et al. 1999); <9 mJy at 12μm and (12 ± 4) mJy at 25 μm (Heckman et al. 1992, near sub–sample).

The dependence on frequency of the FIR flux density in the observed wavelength range 12–200 μm ($\nu_{\rm rest} \approx 36\,000 - 2000$ GHz), can be described by a power law:

$$S(\nu) \propto \nu^{-1\pm0.2}$$

At lower frequencies, however, the spectrum of the FIR component must turn over to meet the 230 GHz upper limit.

This spectrum is clearly not consistent with a single temperature. A multi–temperature fit (as in models by Sanders et al. 1989) would give a plausible range of temperatures between ≈ 25 K and ≥ 120 K in the wavelength range we have considered here. However, as the data quality is not sufficient to allow a meaningful multi–temperature fit, we have taken a simple two temperature approximation, with $T_1 = 80$ K and $T_2 = 25$ K. With corresponding dust masses $M_1 \approx 5\times10^5\ M_\odot$ and $M_2 \approx 2\times10^8 M_\odot$, we can reproduce the FIR flux densities in the range from 60 μm to 200 μm.

Any dust component colder than 25 K is poorly constrained by our data. For instance, up to $10^9\ M_\odot$ would be consistent with the 174/200 μm median flux densities and the 1.3 mm upper limit if the temperature were ≤ 20 K. In order to probe such low temperatures, measures at longer wavelengths would be required, as with SCUBA (Holland et al., 1999). To our knowledge, such data do not exist for our sources.

A comparison of our average mass estimates with those for nearby radio quiet ellipticals (Bregman et al. 1998) and nearby

radio galaxies (Knapp et al. 1990) is not straightforward, as these estimates depend on the wavelengths available and on the assumed temperatures. Bregman et al. (1998) evaluate the temperatures from the 60 μm to 100μm flux density ratio (≈ 30 K) and obtain $10^5 \leq M_{\rm dust}/M_\odot \leq 10^7$. Knapp et al. (1990) assume $T \approx 19$ K and derive $10^6 \leq M_{\rm dust}/M_\odot \leq 10^8$.

In our opinion, it is far from being excluded that the range of dust masses in these samples and in ours are similar, and the different estimates may be due to either the different assumed temperatures and/or to the different wavelength ranges explored.

Using the two temperature approximation, we have also estimated dust masses for the brighter sources detected, or possibly detected, at more than one wavelength.

The results of this calculations are presented in Table 10. Compared to the median values of the total sample, the sources 1345+145, 3C318, 1819+39 and 3C459 seem to have a higher mass of the warm dust component, while the cold dust masses seem to be similar. As the first three objects are a Seyfert type galaxy, a quasar and a Broad Line radio galaxy, we may expect that a favorable orientation of the objects with respect to the line of sight allows us to see the warmer dust associated with the accretion disk.

6.4. What heats the dust?

According to the unification models, the radio galaxies in our sample, which are very powerful in the radio band and have large luminosities in the Narrow Emission Lines ($L_{\rm OIII} \approx 10^{43}$erg s^{-1}, Gelderman & Whittle, 1994), are expected to harbor an obscured quasar (see, e.g., Falcke et al. 1995, in the context of "jet/disk–symbiosis"). A large fraction of the MFIR emission would then originate from the dust in the absorbing torus itself, heated by the UV/X radiation emitted at its center, with some contribution from the interstellar medium, still heated by the central AGN but now distributed over a scale of several kpc, and therefore with temperatures decreasing outwards. We expect this interstellar dust to emit its radiation at the longer wavelengths.

If an obscured AGN is present, adopting a heating model as in Sanders et al. (1989), we expect dust temperatures in a range similar to that estimated in Sect. 6.3.

If, instead, no AGN is present and heating is due to the stellar radiation field only, the dust temperature could be $\lesssim 30$ K, as in nearby radio quiet elliptical galaxies (Bregman et al. 1998). The emission would then peak at $\lambda \geq 200\mu$m. An additional contribution to heating could arise from a burst of star formation, as may be the case in 3C459.

The interpretation based on heating by an obscured quasar is supported by the correlation between radio emission and MFIR emission (Knapp et al. 1990; Heckman et al. 1994), with which our data are also consistent (Fig. 1). Also the strong luminosity in Narrow Lines, which is often interpreted as powered by photo–ionization, gives support to this interpretation. In addition we note that the MFIR average spectrum (for $\lambda_{\rm rest} \geq 20\mu$m) in nearby radio quiet ellipticals (Bregman et al. 1998) is definitely steeper than that of our radio galaxies and of those in Knapp et al. (1990). The spectral index of the former is $\alpha_{\rm RQE} \simeq 2.3 \pm 0.2$, as compared to $\alpha_{\rm us} \simeq 1.0 \pm 0.2$ in our sample (Sect. 6.2) and $\alpha_{\rm Knapp} \simeq 1.2 \pm 0.2$ in Knapp et al. (1990). This suggests that the heating processes are different, with the one in radio galaxies being more effective.

We conclude that our observations are consistent with the MFIR luminosity in these radio galaxies being powered primarily by the AGN, and assume that most of the radiation comes from the "obscuring torus".

6.5. Implications for the circumnuclear torus

Our average FIR luminosities, consistent with the results of Heckman et al. (1992), are about a factor 4 – 5 lower than the FIR luminosities of radio quasars of comparable radio luminosity (see Fig. 2).

This causes problems for the unification models (see Heckman et al. 1992), since, if the torus dust is transparent at FIR wavelengths, its emission should be orientation independent and the quasars should be as luminous in the FIR as the radio galaxies. On the other hand, if the disk is optically thick in some wavelength range, one should justify the constant flux density ratio between radio galaxies and quasars over a broad wavelength range (from 12 to 100 μm).

Hes et al. (1995) discuss the possibility that a beamed non–thermal component is present in quasars and contributes at the FIR wavelengths.

6.6. Back to the frustration scenario for CSS/GPS sources

The original aim of this work was to study the cold phase of the interstellar medium in radio galaxies, in order to see whether its density is high enough to support the "frustration scenario" for CSS/GPS sources. In this scenario, CSS/GPS and large size radio galaxies have similar lifetimes, so that the difference in size (more than a factor of 100, on average, in our two samples, Tables 1 and 2) requires an environment significantly denser for the former (De Young 1993; Fanti et al. 1995).

The hot component of the ISM is too tenuous and has insufficient pressure to confine the radio source (e.g. O'Dea et al. 1996; Readhead et al. 1996). Thus the radio source must be confined via interaction with relatively cold dense material along the path of propagation. However, as anticipated in the introduction, even if a lot of dense cold gas is present in the host galaxy, distributed in the disk/torus of the "unified models" (which is perpendicular to the radio axis) it will have no effect on the radio source propagation. "Frustration", if present, must be due to the diffuse cold phase of the interstellar gas.

From ram pressure computations, the estimates of the density of the interstellar gas required to frustrate CSS radio galaxies imply masses $\geq 2 \times 10^{10}\ M_\odot$ within a volume of ≈ 10 kpc in radius (Fanti et al. 1995), corresponding, for a gas to dust ratio as in our own Galaxy, to an excess dust mass $\geq 2 \times 10^8 M_\odot$. This would produce an excess in the FIR emission of the CSS/GPS, as compared to the large size radio galaxies, the exact amount depending on the dust temperature. The upper limits to any IR

excess derived in Sect. 5.4 convert into an excess dust mass of $\lesssim 0.6\ 10^8 M_\odot$ for $T \gtrsim 30$ K, (if heating is due to a powerful AGN), which is not enough for the frustration model. Even if we attribute the whole MFIR emission we detect from CSS/GPS to a frustrating medium only, and *not* to the dusty disk/torus, the implied mass (for $T \gtrsim 30$ K), would be still not enough, the upper limits to the differences in the MFIR emission being similar to the actual flux densities of CSS/GPS sources.

As a consequence, we may be confident that there is no evidence for a component of the interstellar medium, with temperatures $\gtrsim$30 K, significantly denser or more massive in CSS/GPS galaxies to cause frustration.

For lower temperatures, our FIR observations are not sensitive enough to firmly constrain larger masses, since the emission would peak at $\lambda > 200$ μm, and the uncertainties we have on the flux density limits at long wavelengths are too large to provide safe constraints. For instance, if the temperature were $\approx$20 K, up to $5\times10^8 M_\odot$ of dust would be permitted. This should be probed by observations at longer IR wavelengths (e.g. with SCUBA). An additional strong constraint on such large dust masses is obtained from the color properties of the host galaxies. Dust masses as required by frustration, spread over ~ 10 kpc, would produce absorption in the optical band. The implied hydrogen column density, $N_{\rm H} \geq 10^{22}$ g cm^{-2}, corresponds to an optical depth in the visual $\tau_{\rm v} \approx N_{\rm H}/(2\ 10^{21})$. Applying a model of homogeneously mixed dust and stars (as in Goudfrooij & de Jong 1995), the above dust mass implies $A_{\rm v} \approx 2$ mag., and color reddening E(B–V) ≈ 0.7, which is inconsistent with the data of de Vries et al. (1998).

If "frustration" occurs only for GPS (sizes ≤ 1 kpc), the implied masses are lower, but their temperature would be larger (≥ 50 K, for a model as in Sanders et al. 1989), due to the closer proximity to the hidden quasar, so that the expected IR luminosity would be even more discrepant with what we observe.

The present conclusion is therefore that the FIR radiation we detect with ISO does not imply an amount of gas (heated by the AGN) large enough to support the frustration scenario of CSS/GPS radio sources. This is consistent with the results of Owsianik et al. (1998) and Owsianik & Conway (1998), who found fast proper motions of the outer lobes in some small symmetric GPS, and with the radio spectra analysis of CSS/GPS by Murgia et al. (1999).

We finally note that recent observations with SCUBA (Archibald et al. 2000) of high redshift radio galaxies, both CSS and large size ones, do not show any significant difference between the two classes of sources.

The MFIR properties of CSS/GPS, however, point out a new problem for the alternative interpretation. An important ingredient of the "youth scenario" is that the radio luminosity is required to decrease with increasing source size, in order to explain the numerical proportion of CSS/GPS to large size sources. In the current models, this luminosity evolution is essentially due to expansion of the lobe volumes in an external medium of decreasing density and not to a decline of the power carried by the jet with time. CSS/GPS sources would evolve, with increasing size, toward lower luminosity larger size radio sources. This evolution in luminosity may also be described in terms of a higher efficiency for converting the beam power into radio band radiation (see also Gopal & Wiita 1991) in the early phases of the source evolution.

According to this idea, our two samples (CSS/GPS and comparison), which have very different sizes but similar radio luminosities, would have "radio engines" of power different by a factor 10 or so (CSS/GPS being less powerful). As in the past there have been strong suggestions that the jet power is proportional to the bolometric luminosity of the AGN (e.g. Baum & Heckman 1989; Rawlings & Saunders 1991; Falcke et al. 1995), one would expect the CSS/GPS to be definitely less powerful in the MFIR (and in the NL emission). This is not seen in our observations, at least at 60 and 90 μm.

Although we have no obvious solution to this problem, we speculate here about a couple of possibilities. First there may be an additional source of heating arising from conversion of a fraction of the jet power where the jet interacts with the interstellar medium. This may be more effective at distances close to the nucleus and less so further out as the source ages. The existence of emission line gas aligned with the radio source in low redshift CSS sources is consistent with strong interaction between GPS/CSS sources and the dense clouds in the ISM (de Vries et al. 1999). Such an effect should roughly compensate for the lower radiation power from the central engine in CSS/GPS.

The second possibility is related to the scenario where the radio emission is triggered by a merger event. We speculate that in the early phase of the radio source life a large fraction of gas/dust is not fully settled in a disk/torus but is still distributed over a much larger solid angle, as seen from the central continuum source. In this scenario the fraction of intercepted and reprocessed UV radiation could be much higher in the younger/smaller sources, increasing their MFIR emission. We might also expect the additional obscuration in the smaller sources to result in lower emission line luminosities and/or redder colors. This is not generally seen in GPS and CSS sources, though there are a few cases which are consistent with this picture (O'Dea 1998; de Vries et al. 1998). In addition, this hypothesis would require the gas/dust to settle into a disk on a timescale much less than the age of a radio source (10^{7-8} yr) in order to remove the extra obscuration before the sources propagate to scales larger than tens of kpc.

At present, both of these explanations appear rather "ad hoc". Thus, this issue remains a problem for the current evolution models.

7. Conclusions

a) We have presented ISOPHOT observations at $\lambda = 60$, 90, 174 and 200 μm of CSS/GPS radio galaxies and of a matched comparison sample of extended radio galaxies. A minority of objects are detected individually at one or more wavelengths in both samples.

b) We have co–added the data for each sample to obtain mean and median flux densities. The extrapolated radio spec-

trum under–predicts the observed MFIR flux densities, arguing that the MFIR is due to dust rather than to synchrotron emission.

c) We find no significant differences in the MFIR flux densities of the two samples. Our results are then consistent with the CSS/GPS and the extended radio galaxies having similar MFIR luminosities. For dust temperatures $\gtrsim$30 K, the deduced masses of the interstellar gas are lower than required by the frustration scenario. For lower temperatures larger masses would be allowed for by our data, but they would produce a large amount of obscuration and reddening in the optical, which is not seen in the existing data.

All this argues against the CSS/GPS sources being "frustrated" by a dense ambient medium.

d) Since no significant difference is seen between the two samples, we have combined them for further analysis. The average $L_{\rm FIR}$ is in the range $(0.6-1.0)\times10^{11}$ L$_\odot$ or $(2-5)\times10^{44}$ erg s^{-1}. Over the wavelength range of our observations, the spectrum can be fitted by a single power law with $\alpha \simeq 1.0\pm0.2$.

e) We have fitted simple two temperature ($T_1 = 80$ K and $T_2 = 25$ K) models to the IR spectrum and have derived dust masses of $M_1 \approx 5\times10^5\ M_\odot$ and $M_2 \approx 2\times10^8 M_\odot$. The mass of the cold dust appears higher than found in radio quiet elliptical galaxies, although this difference may be due to the differences in the assumed temperatures and the sampled rest-frame wavelength coverage.

f) Our observations are consistent with the MFIR luminosity in these powerful radio galaxies being mostly powered by an obscured AGN, although in some objects a contribution from star formation is possible.

Acknowledgements. We are grateful to Dr. M. Haas of MPIA (Heidelberg) for his numerous suggestions during the data analysis stage and for providing us with specialized software to perform some non standard data reduction. CF and FP wish also to thank MPIA staff members for the help obtained during a short visit at the ISOPHOT group in Heidelberg.

This work was partly supported by the Italian Ministry for University and Research (MURST) under grant cofin99-02-32

References

Allen R.J., Le Bourlot J., Lequeux J., et al., 1995, ApJ 444, 157
Archibald E.N., Dunlop J.S., Hughes D.H., et al., 2000, MNRAS, in press
Baum S.A., Heckman T., Bridle A., et al., 1988, ApJS 68, 643
Baum S.A., Heckman T., 1989, ApJ 336, 702
Bicknell G.V., Dopita M.A., O'Dea C.P., 1997, ApJ 485, 112
Bregman J.N., Snider B.A., Grego L., et al., 1998, ApJ 499, 670
Desert F.X., Boulanger F., Puget J.L., 1990, A&A 237, 215
de Vries W.H., O'Dea C.P., Baum S.A., et al., 1998, ApJ 503, 156
de Vries, W.H., O'Dea C.P., Baum S.A., et al., 1999, ApJ 526, 27
De Young D.S., 1993, ApJ 402, 95
Evans A.S., Kim. D.C., Mazzarella J.M., et al., 1999, ApJ 521, L107
Falcke H., Malkan M.A., Biermann P.L., 1995, A&A 298, 375
Falco E.E., Impey C.D., Kochanek C.S., et al., 1999, ApJ 523, 617
Fanti R., Fanti C., Schilizzi R.T., et al., 1990, A&A 231, 333
Fanti C., Fanti R., Dallacasa D., et al., 1995, A&A 302, 317
Fosbury R.A., Mebold U., Goss W.M., et al., 1977, MNRAS 179, 89
Fosbury R.A., Bird M.C., Nicholson W., et al., 1987, MNRAS 225, 761
Gabriel C., Acosta–Pulido J., Heinrichsen I., et al., 1997, In: Huntn G., Payne H.E. (eds.) Proc. of the ADASS VI Conference, ASP Conf. Ser. vol 125, p. 108
Gautier III T.N., Boulanger F., Perault M., et al., 1992, AJ 103, 1313
Gelderman R., Whittle M., 1994, ApJS 91, 491
Gilmore G.F., Shaw H.A., 1986, Nat 321, 750
Golombek D., Miley G.K., Neugebauer G., 1988, AJ 95, 26
Gopal K., Wiita P., 1991, ApJ 373, 325
Goudfrooij J.S., de Jong T., 1995, A&A 298, 784
Goudfrooij P., de Jong T., Hansen L., et al., 1994, MNRAS 271, 833
Heckman T.M., Smith E.P., Baum S.A., et al., 1986, ApJ 311, 526
Heckman T.M., Chambers K.C., Postman M., 1992, ApJ 391, 39
Heckman T.M., O'Dea C.P., Baum S.A., et al., 1994, ApJ 428, 65
Hes R., Barthel P.D., Hoekstra H., 1995, A&A 303, 8
Hildebrand R.H., 1983, QJRAS 24,267
Holland W.S., Robson E.I., Gear W.R., et al., 1999, MNRAS 659
Hughes D.M., Dunlop J.S., Rawlings S.R., 1997, MNRAS 289, 766
Hurt T., Antonucci R., Cohen R., et al., 1999, ApJ 514, 579
Impey C., Gregorini L., 1993, AJ 105 853
Jauncey D.L., White G.L., Batty M.J., et al., 1986, AJ 92, 1036
Kessler M.F., Steinz J.A., Anderegg M.E., et al., 1996, A&A 315, L27
Knapp G.R., Bies W.E., van Gorkom J.H., 1990, AJ 99, 476
Kuncic Z., Bicknell G.G., Dopita M.A., 1998, ApJ 495, L35
Laing R.A., Riley J.M., Longair M.S., 1983, MNRAS 204, 151 (**3CR)**
Lemke D., Klaas U., Abolins J., et al., 1996, A&A 315, L64
Mirabel I.F., Sanders D.B., Kazès I., 1989, ApJ 340, L9
Morganti R., Tadhunter C.N., Dickson R., et al., 1997, A&A 326, 130
Murgia M., Fanti C., Fanti R., et al., 1999, A&A 345, 769
Neugebauer G., Miley G.K., Soifer B.T., et al., 1986, ApJ 308, 815
O'Dea C.P., 1998, PASP 110, 493
O'Dea C.P., Baum S.A., Maloney P.R., et al., 1994, ApJ 422, 467
O'Dea C.P., Worrall D.M., Baum S.A., et al., 1996, AJ 111, 92
O'Dea C.P., de Vries W.H., Worrall D.M., et al., 2000, AJ 119, 478
Owsianik I., Conway J.E., 1998, A&A 337, 69
Owsianik I., Conway J.E., Polatidis A.G., 1998, A&A 336, L37
Peacock J.A., Wall J.V., 1982, MNRAS 198, 843 (**PW**)
Phillips R.B., Mutel R.L., 1982, A&A 106, 21
Rawling S., Saunders R., 1991, Nat 349 438
Readhead A.C.S., Taylor G.B., Xu W., et al., 1996, ApJ 460, 612
Sanders D.B., Soifer B.T., Elias J.H., et al., 1988, ApJ 328, L35
Sanders D.B., Phinney E.S., Neugebauer G., et al., 1989, ApJ 347, 29
Sanghera H.S., Lüdke D.J., Spencer R.E., et al., 1995, A&A 295, 629
Savage A., 1976, MNRAS 174, 259
Snellen I.A.G., Schilizzi R.T., De Bruyn A.G., et al., 1998, A&AS 131, 435
Snellen I.A.G., Schilizzi R.T., Bremer M.N., et al., 1999, MNRAS 307, 149
Spinrad H., Smith H.E., 1976, ApJ 206, 355
Spinrad H., Djorgovski S., Marr J., et al., 1985, PASP 97, 932
Stanghellini C., O'Dea C.P., Baum S.A., et al., 1997, A&A 325, 943
Stanghellini C., O'Dea C.P., Dallacasa D., et al., 1998, A&AS 131, 303
Surace J.A., Sanders D.B., Vacca W.D., et al., 1998, ApJ 492, 116
Tadhunter C.N., Shaw M.A., Morganti R., 1994, MNRAS 271, 807
Taylor G.B., Inoue M., Tabara H., 1992, A&A 264, 421
Tingay S.J., Jauncey D.L., Reynolds J.E., et al., 1997, AJ 113, 2025
Tzioumis A.K., King E.A., Jauncey D.L., et al., 1997, In: Snellen I.A.G., Schilizzi R.T., Röttgering H.J.A., Bremer M.N. (eds.) The Second Workshop on CSS/GPS Radio Sources. p. 67

Ulvestad J.S., 1985, ApJ 288, 514
van Breugel W.J.M., Heckman T., Miley G.K., 1984, AJ 89, 5
Veilleux S., Sanders D.B., Kim D.-C., 1997, ApJ 484, 92
Vermeulen R.C., Taylor G.B., Readhead, A.C.S., 1996, AJ 111, 1013
Veron–Cetty P.P., Woltjer L., Ekers R.D., et al., 1995, A&A 297, L79
Willott C.J., Rawlings S., Jarvis M.J., 2000, MNRAS 313, 237

Note added in proof: About the comparison between FIR luminosities of radio loud quasars and radio galaxies, very recent ISO observations by Müller et al. (2000) (workshop "FIRSED 2000", Groningen, April 27–29, 2000; ed. P.Barthel et al.), show no difference between the two classes of objects, contrary to what found by Heckman et al. (1992), shown in Fig. 2 and commented in Sect. 6.5.